# Alternative Fuel Technologies

This paper is published as part of the high-profile series of PCCP special issues on Alternative Fuel Technologies.

Guest edited by Joachim Maier (MPI Stuttgart), Dirk Guldi (Universität Erlangen-Nürnberg), and Adriano Zecchina (University of Torino), and published in selected 2007 print issues of PCCP, all papers are collected online on a dedicated website:

**www.rsc.org/pccp/altfuel**

Visit the website for both cutting edge research papers and authoritative review articles by leaders in a range of fields of critical importance to the world today

- fuel cells
- electrochemical energy conversion
- supercapacitors and molecular materials
- hydrogen storage
- solar energy conversion
- biohydrogen

Sign up for RSS alerts to have the latest articles delivered directly to your desktop

RSC Publishing

www.rsc.org/pccp/altfuel

Registered Charity Number 207890

# Dye-sensitized nanocrystalline solar cells

**Laurence M. Peter***

***Received 22nd November 2006, Accepted 3rd January 2007***
***First published as an Advance Article on the web 25th January 2007***
**DOI: 10.1039/b617073k**

The basic physical and chemical principles behind the dye-sensitized nanocrystalline solar cell (DSC: also known as the Grätzel cell after its inventor) are outlined in order to clarify the differences and similarities between the DSC and conventional semiconductor solar cells. The roles of the components of the DSC (wide bandgap oxide, sensitizer dye, redox electrolyte or hole conductor, counter electrode) are examined in order to show how they influence the performance of the system. The routes that can lead to loss of DSC performance are analyzed within a quantitative framework that considers electron transport and interfacial electron transfer processes, and strategies to improve cell performance are discussed. Electron transport and trapping in the mesoporous oxide are discussed, and a novel method to probe the electrochemical potential (quasi Fermi level) of electrons in the DSC is described. The article concludes with an assessment of the prospects for future development of the DSC concept.

## Introduction

The history[1] of dye-sensitization of wide bandgap semiconductors can be traced as far back as 1873, the date of Hermann Wilhelm Vogel's accidental discovery that contamination of silver halide photographic emulsion by a green dye† made the film much more sensitive to red light. Only a year later, Sir William de Wiveleslie Abney had already achieved sensitization of photographic emulsion throughout the entire optical solar spectrum, from violet to infrared. A century later, the application of sensitization to photoelectrochemical systems[2] was the subject of widespread research, particularly in the sixties and seventies,[3,4] when it was established that the sensitization process involved electron (or hole) injection from the excited state of the sensitizer dye rather than energy transfer. However, at this time there seemed little scope for practical application of the effect to solar energy conversion, since the currents generated by sensitization of single crystal electrodes such as zinc oxide are very small because the dye is present only as a monolayer at the surface and light absorption is therefore very weak. However, in 1976 Tsubomura *et al.*[5] demonstrated that larger photocurrents could be obtained by replacing the flat surface of a single crystal of ZnO by a porous microcrystalline layer, thereby increasing the surface area of the semiconductor to enhance light harvesting. Interestingly, it was not this paper in *Nature* that led to the explosion of interest in dye-sensitized solar cells (DSC). Instead, this was stimulated fifteen years later by the much-cited‡ *Nature* paper of O'Regan and Grätzel,[6] who showed that an efficient (>7%) regenerative photoelectrochemical solar cell could be fabricated using a mesoporous layer of titanium dioxide sensitized by a strongly absorbed ruthenium dye. Since then, efforts to optimize DSC have resulted in cells with AM 1.5§ efficiencies above 11%,[7] and the technology is now approaching the stage where it is poised to compete with more conventional photovoltaics. New developments include the use of templated mesoporous $TiO_2$ layers[8,9] and new organic dyes.[10–14] At the same time, the understanding of processes occurring on the nanoscale developed by research on DSCs will increasingly be applied to other devices for solar energy conversion, including organic bulk heterojunction solar cells,[15–18] hybrid organic/inorganic solar cells[19–21] and tandem water splitting systems for solar hydrogen generation.[22,23]

Fabrication of a typical DSC starts with two sheets of glass coated with a transparent layer of fluorine-doped tin oxide. One plate is coated with a thin layer of colloidal $TiO_2$ paste consisting of particles with sizes in the 20–40 nm range. The film is sintered in air at 400 °C to produce a mesoporous layer ($\approx$10 μm) with a porosity of around 50%, which is then sensitized by adsorption of a dye such as the widely-used *cis*-bis(isothiocyanato) bis(2,2′-bipyridyl-4,4′-dicarboxylato)-ruthenium(II) bis-tetrabutylammonium[24,25] (Fig. 1) or one of the recently introduced organic dyes.[14,26,27]

The second glass plate is coated with a thin film of platinum by sputtering or by electrochemical deposition. The two plates are sandwiched together with hot melt polymer gasket, and an electrolyte consisting of the iodide/tri-iodide redox couple in a suitable solvent is filled through a small hole drilled in the platinum coated plate, which is then sealed. The steps in the assembly are illustrated in Fig. 2.

Generation of a photocurrent in the DSC occurs when light is absorbed by the sensitizer dye, resulting in ultra-fast electron injection into the conduction band of the $TiO_2$.[28–31] The injected electrons move through the network of interconnected

*Department of Chemistry, University of Bath, Bath, UK BA2 7AY. E-mail: l.m.peter@bath.ac.uk*

† The green dye was applied to the back of photographic plates to reduce reflection.

‡ Over 2700 citations at the time this review was written.

§ AM 1.5 (air mass 1.5) refers to standard solar irradiance at the surface of the earth at an angle of incidence of 48° relative to the surface normal.

 This journal is © the Owner Societies 2007

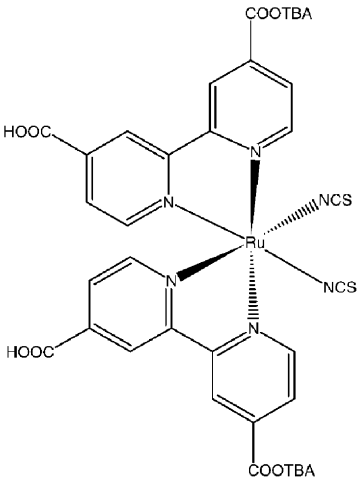


**Fig. 1** Structure of the most commonly used ruthenium dye employed to sensitize the high surface area $TiO_2$ layer in the dye-sensitized solar cell.

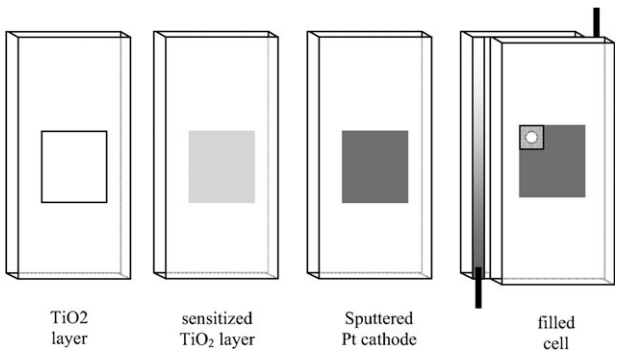


**Fig. 2** Fabrication of a dye sensitized mesoporous solar cell.

oxide particles (typical size 30–40 nm) by a random walk process[32] until they reach the conducting glass substrate¶. The oxidized dye is regenerated by rapid electron transfer from the iodide ions in the electrolyte before it has time to undergo irreversible bleaching.[33,34] The $I_3^-$ ions produced in the regeneration step diffuse the short distance (typically $<40$ μm) to the platinum-coated cathode, where they are reduced to iodide ions to complete the regenerative cycle. The dye regeneration step is analogous to the super-sensitization process that is used in photography to allow dye molecules to inject electrons repeatedly without bleaching. A recent estimate suggests that turnover numbers‖ in excess of $10^8$ are feasible in the DSC, giving a lifetime of 20 years or more.[7] The timescale on which processes in the DSC occur ranges from sub-picoseconds for electron injection to seconds for diffusion of redox ions between the two plates. The complete regenerative cycle is illustrated schematically in Fig. 3.

¶ The electrons undergo multiple trapping as they move to the contact. This is discussed later.

‖ In a DSC under 1 sun illumination, each dye molecule absorbs photons at a rate of about 1 per second, corresponding to $3.2 \times 10^7$ turnovers per year.

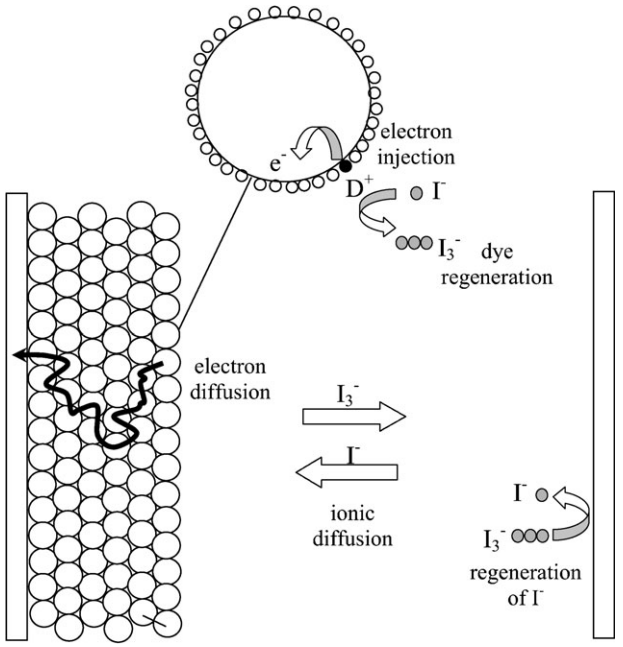


**Fig. 3** Summary of the processes taking place during the regenerative cycle in the dye-sensitized cell.

## Basic principles

### Free energy and driving forces

The energetics of the DSC are usually discussed in terms of the relative positions of the energies of the $TiO_2$ conduction band, the HOMO/LUMO energies of the dye and the 'redox energy' of the $I_3^-/I^-$ couple, as illustrated in Fig. 4. For successful sensitization, the dye LUMO level must be higher in energy than the conduction band of the $TiO_2$, whereas the redox energy must be higher than the HOMO level to allow regeneration of the dye from its oxidized state.

While Fig. 4 is helpful for the purpose of visualizing the processes in the DSC, it is misleading when used to understand the energetics of the cells because it mixes potential energy (*e.g.* conduction band energy) and free energy (redox energy)

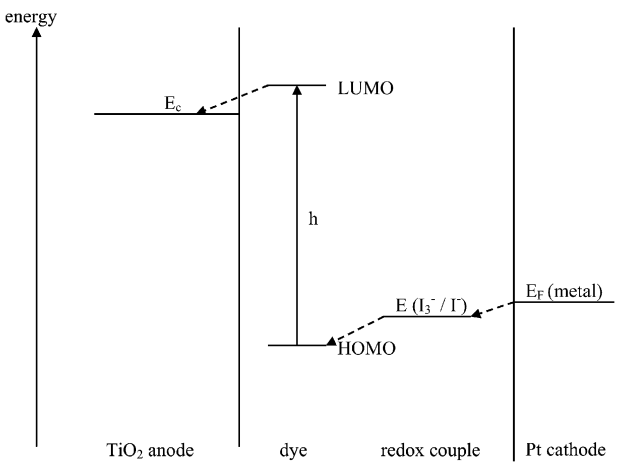


**Fig. 4** Energy levels in the dye-sensitized solar cell.

scales. A similar problem arises in the description of the photovoltaic cell found in many elementary texts, where the driving force for the separation of electrons and holes is incorrectly identified with the electrostatic potential difference (*i.e.* potential energy) across the p–n junction. In fact, the free energy of electrons and holes is sensitive not only to changes in their potential energy arising from the electrical potential, but also to their concentration (*via* the entropic term in the Gibbs energy). The driving force for the movement of charge carriers is the gradient of free energy (which is small in a typical silicon solar cell) and not the gradient of potential energy (which can be large in a p-n junction).

Würfel[35] has shown with remarkable clarity that many apparently different types of devices for converting solar energy share at least two common elements—a light absorbing material and membrane-like contacting phases that are selective for either electrons or holes. Absorption of light in the absorber creates electron–hole pairs that have different free energies. This separation of free energies is a measure of the energy available internally in the device. The role of the contacts is to allow as much as possible of this free energy separation to be available at the contacts as a voltage. In a p-i-n solar cell, the p- and n- contacts are selective for holes and electrons, respectively. Selectivity is achieved in the DSC by using different electron and hole conducting phases. The selectivity is not ideal however, since whereas there is a large thermodynamic barrier for hole injection into the $TiO_2$ from the redox electrolyte, electron injection into the $I_3^-/I^-$ electrolyte from the $TiO_2$ is energetically 'downhill' and associated with a kinetic barrier that arises from the activation energy required to break the I–I bond in the process.

The driving force for transport of electrons and holes (or any other species such as ions) in any solar cell is the gradient of free energy or electrochemical potential, $\bar{\mu}_i$. In solid state physics, the electrochemical potential is identified with the Fermi energy, $E_F$. In general, the electrochemical potential $\bar{\mu}_i$, associated with a species $i$ with charge $z_i q$ is defined as

$$\bar{\mu}_i = \mu_i^0 + k_B T \ln \frac{n_i}{n_i^0} + z_i q \varphi \qquad (1)$$

where $\varphi$ is the inner potential, $n_i$ is the density of the species and $n_1^0$ is the density of the appropriate reference state for which the chemical potential takes its standard value $\mu_i^0$. In general terms, the flux of any charged species is related to the gradient of free energy by the expression

$$J_i = -\frac{z_i n_i u_i}{q} \frac{\partial \bar{\mu}_i}{\partial x} \qquad (2)$$

where $u_i$ is the mobility. The gradient of electrochemical potential can be found from eqn (1):

$$\frac{\partial \bar{\mu}_i}{\partial x} = \frac{k_B T}{n_i} \frac{\partial n_i}{\partial x} + z_i q \frac{\partial \varphi}{\partial x} \qquad (3)$$

It follows that the flux of species is given by

$$J_i = -\frac{u_i k_B T}{q} \frac{\partial n_i}{\partial x} - z_i u_i n_i \frac{\partial \varphi}{\partial x} \qquad (4)$$

Using the Einstein relation $D_i = \frac{kT}{q} u_i$, which relates the diffusion coefficient $D_i$ to the mobility, we obtain

$$J_i = -D_i \frac{\partial n_i}{\partial x} - z_i n_i u_i \frac{\partial \varphi}{\partial x} \qquad (5)$$

The first term is familiar as Fick's first law of diffusion. The second term represents the migration or drift flux. The more general expression given by eqn (2) will be utilized here, since the gradient of electrochemical potential corresponds to the gradient of the Fermi level used in semiconductor physics.

In a conventional silicon solar cell, only small gradients of free energy are required to drive the short circuit currents because the mobilities of holes and electrons in the highly pure material are high (400–1000 $cm^2\ V^{-1}\ s^{-1}$). In the DSC, the mobile charges are electrons in the $TiO_2$ and either tri-iodide ions in electrolyte-based cells or holes (radical cations) in cells in which the electrolyte has been replaced with an organic hole conductor such as 2,2′,7,7′-tetrakis(*N*,*N*-di-*p*-methoxyphenylamine)9,9′-spiro-bifluorene (OMeTAD).[36,37] The mobility of free electrons in $TiO_2$ is two orders of magnitude smaller than in pure silicon, and the mobilities of ionic species in the redox electrolyte (or holes in an organic hole conductor) are at least six orders of magnitude smaller. This means that larger gradients of free energy are required to support current densities (typically 15–20 mA $cm^{-2}$) generated by solar radiation. In addition, substantial free energy differences may be required to drive interfacial electron transfer processes in the DSC. Both electron transport and electron transfer are dissipative processes, leading to efficiency losses.

### The role of electrical fields

It is often stated that the 'built in field' is essential in a p-n junction solar cell since it is needed to separate photogenerated electrons and holes. The preceding discussion was intended to show that this is incorrect. The driving force for separation is in fact the gradient of free energy or of the *quasi-Fermi levels*** for electrons and holes. This raises the question whether electrical fields and 'built in potentials' are important in the DSC. We begin by considering what happens when an isolated nanocrystalline particle of $TiO_2$ is brought into contact with the redox electrolyte. For the calculations that follow, we assume that the particle has a radius of 20 nm and is doped n-type with oxygen vacancies with a density of $10^{18}$ $cm^{-3}$. The Fermi level in the particle before immersion is close to the conduction band, and in the absence of other sources of charge, the particle is electrically neutral since the densities of conduction and electrons and ionized donor states are equal. Several estimates indicate that the Fermi energy of the $I_3^-/I^-$ couple is located around 1 eV below the conduction band of the $TiO_2$ as shown in Fig. 5. Consequently, electrons will be extracted from the n-doped particle until the Fermi levels are equilibrated. This will leave the particle with a net positive charge associated with the ionized donors in the lattice. If the particle is small, the density of ionized donor states will now exceed that of the electrons by many orders of

** The term quasi Fermi level is used in solid state physics to describe systems in which electrons and holes are in thermal equilibrium with the lattice but not with each other. This is the situation under steady illumination, where a photostationary state is produced.


This journal is © the Owner Societies 2007

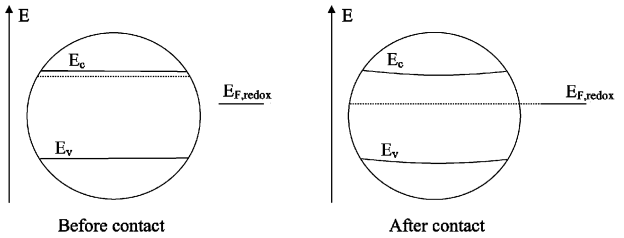


**Fig. 5** Equilibration of Fermi levels between a $TiO_2$ particle and the $I_3^-/I^-$ redox electrolyte in the dark. Note that the band bending induced in the particle is small (< 50 meV) unless the doping density is higher than $10^{18}$ $cm^{-3}$.

magnitude, and the particle is fully depleted. The electrical field is readily found by solving Poisson's equation in spherical coordinates.

$$\frac{\partial^2\phi}{\partial r^2} - \frac{2}{r}\frac{\partial\phi}{\partial r} = -\frac{\rho}{\varepsilon\varepsilon_0} = -\frac{qN_d}{\varepsilon\varepsilon_0} \qquad (6)$$

For a particle with radius $R$, the solution†† is

$$\phi(r) = \frac{qN_d}{6\varepsilon\varepsilon_0}[R^2 - r^2] + \frac{qN_d}{3\varepsilon\varepsilon_0}R^2 \qquad (7)$$

and the variation of electrical potential leads to a distortion of the energies of the conduction and valence bands illustrated in Fig. 5.

In the case where the doping density is $10^{18}$ $cm^{-3}$, there is a 'band bending' of 40 meV between the centre of the particle and the surface (it is exaggerated in the figure to make it visible). Note that this is more than an order of magnitude smaller than the initial difference in Fermi levels (around 1 eV). If the doping level is $10^{17}$ $cm^{-3}$, the band bending inside the particle is reduced to only 4 meV.

Since the Fermi energy is the same throughout the particle, the change in electrical potential is offset by a corresponding variation of electron density. This means that at equilibrium in the dark, the ratio of the electron density at the surface of the particle to the density at the centre will be given by

$$\frac{n(r=R)}{n(r=0)} = \exp -\frac{q\phi_R}{k_B T} \qquad (8)$$

For the present case ($R$ = 20 nm, $N_d = 10^{18}$ $cm^{-3}$, $T$ = 300 K, the ratio is 0.2, *i.e.* the surface is weakly depleted relative to the centre. For lower doping densities, the difference becomes insignificant, and the interior of the particle can be treated as field free. Interestingly, the influence of band bending is expected to become important for higher doping densities, when it could lead to electron channelling as illustrated in Fig. 6 for an array of interconnected spherical particles. One can speculate that by keeping photogenerated electrons near the centre of the 'channels', losses due to back reaction with $I_3^-$ could be reduced. The effect should be most marked in the case of highly doped particles or large particles.

†† The arbitrary zero of potential has been taken as in vacuum at infinity.

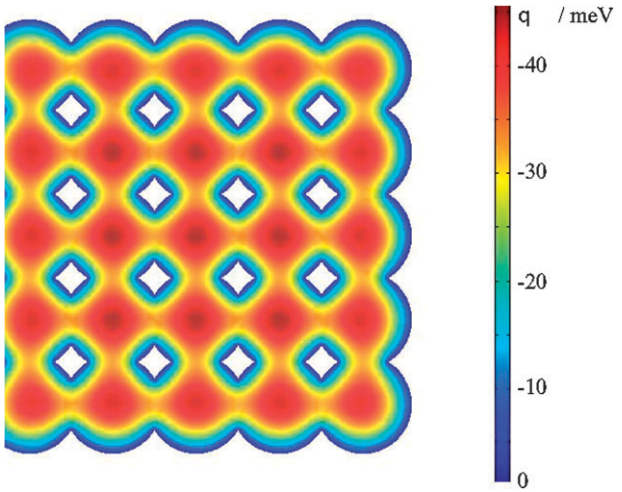


**Fig. 6** Band bending in an array of sintered spherical $TiO_2$ particles (radius 20 nm, doping density $10^{18}$ $cm^{-3}$). The maximum band bending is 40 meV. The band bending could assist in the channelling of electrons to the contact.

## Contacting the nanocrystalline oxide

On the basis of this analysis, we may expect an ensemble of interconnected $TiO_2$ particles immersed in the redox electrolyte to be completely depleted (and hence insulating) in the dark. In the DSC, however, the last layer of oxide nanoparticles is in contact with the conducting glass substrate, so we need to consider the nature of this junction. We begin by assuming that the nanocrystalline layer is deposited directly on the fluorine doped tin oxide glass coating (*i.e.* there is no intermediate or 'blocking' layer). Consider an isolated particle of $TiO_2$ that is brought into contact with the $SnO_2$(F). Depending on the relative positions of the Fermi levels in the two materials, equilibration of electrons at the contact may lead to depletion of the $TiO_2$ or of the $SnO_2$. For simplicity, we will assume that the Fermi levels are equal before contact, although this does not change the following argument. The electron affinity of $SnO_2$ is believed to be about 0.3 eV greater than that of $TiO_2$, and this difference has been incorporated in the band diagram shown in Fig. 7. The junction is then brought into contact with the redox electrolyte to form a three phase contact, resulting in a downward movement of the Fermi levels. The situation after contact is illustrated in Fig. 7. It can be seen that band bending in the $SnO_2$(F) is large,

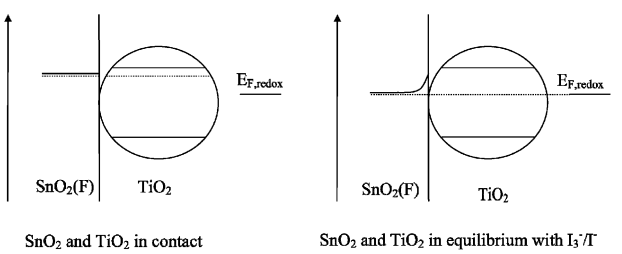


**Fig. 7** Band bending at the contact between the $TiO_2$ layer and the $SnO_2$(F)-coated conducting glass substrate. Note that equilibration of the Fermi levels in the dark induces a depletion layer in the $SnO_2$.

whereas by contrast the band bending in the particle is too small to be visible in the figure.

It is important to note that in the absence of a blocking layer, the underlying $SnO_2$(F) is not only in contact with the nanoparticles but also directly with the redox electrolyte. In these uncoated areas, the $SnO_2$ will also be depleted in the same way. The width of the space charge layer formed in the highly doped ($\approx 10^{20}$ cm$^{-3}$) $SnO_2$(F) coating is given by

$$W_{sc} = \left(\frac{2\Delta\phi\varepsilon\varepsilon_0}{qN_d}\right)^{1/2} \quad (9)$$

where $\Delta\phi$ is the potential difference across the space charge region, $\varepsilon$ is the relative permittivity of $SnO_2$ and $\varepsilon_0$ is the permittivity of free space. $W_{sc}$ is therefore only a few nm, so that electrons will be able to tunnel readily across the barrier. This means that as far as electrochemical processes are concerned, the $SnO_2$(F) layer behaves like a metal electrode. We can conclude that there is indeed a 'built in potential'. However, it is not located in the mesoporous film but at the substrate interface. Consequently, electron transport in the bulk of the mesoporous film is expected to occur by diffusion.

### Open circuit voltage of the DSC

We begin by considering the situation where the DSC is illuminated at open circuit. Under these conditions, injection of electrons from photoexcited dye molecules must be balanced by the sum of all routes for electron transfer in the opposite direction. Three such routes can be identified. The first is transfer of electrons from the mesoporous $TiO_2$ layer to $I_3^-$ ions in the electrolyte‡‡. The second is transfer of electrons from the mesoporous oxide to oxidised dye molecules attached to the surface, and the third is electron transfer to $I_3^-$ ions *via* the $SnO_2$(F) contact. The rate of electron injection is determined by the light intensity and the surface coverage of adsorbed dye. Light scattering can be neglected if the $TiO_2$ particles are sufficiently small, and the local rate of electron injection $\upsilon_{inj}(\lambda, x)$ can be calculated using the expression for an isotropic non-scattering optical medium

$$\upsilon_{inj}(\lambda, x) = \eta_{inj}\alpha(\lambda)I_0 e^{-\alpha x} \quad (10)$$

where $\eta_{inj}$ is the efficiency of electron injection from the excited state of the dye. The absorption coefficient, $\alpha$, is related to the effective molar concentration $c$ and molar absorption coefficient $\varepsilon(\lambda)$ of the dye

$$\alpha(\lambda) = 2.303\varepsilon(\lambda)c \quad (11)$$

The rate of reverse electron transfer from the nanocrystalline $TiO_2$ to the oxidized dye is determined by competition between the reaction

$$D^+ + e^-_{TiO_2} \rightarrow D \quad (12a)$$

and the regeneration step

$$D^+ + I^- \rightarrow D + I^{-\bullet} \quad (12b)$$

Under steady state conditions, the rate of electron transfer to $D^+$ is given by

$$\upsilon_{D^+} = \upsilon_{inj}\left(\frac{k_{D^+}n}{k_{D^+}n + k_{reg}[I^-]}\right) \quad (13)$$

The concentration of iodide ions in the DSC is usually sufficiently high ($>10^{20}$ cm$^{-3}$) that reaction (12a) can be neglected to a first approximation.

The rate of electron transfer to $I_3^-$ ions is the dominant quantity that determines the open circuit voltage at high intensities of the order of 1 sun. In the absence of dissociative chemisorption of iodine, the first step in the reduction

$$I_3^- + e^-_{TiO_2} \rightarrow I^- + I_2^{-\bullet} \quad (14a)$$

can be followed either by a second electron transfer step

$$I_2^{-\bullet} + e^-_{TiO_2} \rightarrow zI^- \quad (14b)$$

or by the reaction

$$2I_2^{-\bullet} \rightarrow I_3^- + I^- \quad (14c)$$

If the step (14a) is rate-determining, the expression for the rate of 'recombination'§§ takes the form

$$\upsilon_{I_3^-} = k_{I_3^-}n[I_3^-] \quad (15)$$

This rate expression will also be valid if the mechanism involves dissociation of $I_2$ prior to electron transfer,[38] with the rate constant incorporating the equilibrium constant for dissociation.

The third route by which electrons can react involves transfer from the $SnO_2$(F) substrate to $I_3^-$. We can treat this as an electrochemical process using Butler Volmer kinetics.[39] The driving force for the reaction comes from the overpotential—the difference between the potential of an electrode and its equilibrium (Nernstian) potential. In the open circuit case, the potential of the $SnO_2$(F) electrode is changed under illumination by an amount corresponding to the open circuit voltage. In the dark, the electrode potential is equal to the equilibrium potential of the $I_3^-/I^-$ couple, so the magnitude of the overvoltage under illumination is equal to the photovoltage. The current density associated with reaction (14) can therefore be written as[40,41]

$$j_{sub} = j^0_{sub}\left[\exp\left(\frac{-(1-\alpha)qU_{photo}}{k_BT}\right) - \exp\left(\frac{\alpha qU_{photo}}{k_BT}\right)\right] \quad (16)$$

(note that a reduction current is taken to have a negative sign, whereas the photovoltage is taken as a positive quantity). Here $j^0_{sub}$ is the exchange current density, which depends on the standard rate constant for electron transfer $k^0$ and the concentrations of the redox components.[39] The key point here is that additional current flows internally *via* the substrate, even though the cell is at open circuit.

The open circuit condition can now be defined in terms of the injection rate and the recombination rates for all three

‡‡ This electron transfer can occur either directly from the conduction band or *via* surface states in the bandgap. The analysis of the latter case is complex and outside the scope of this review.

§§ The term 'recombination' usually refers to electron–hole recombination in semiconductors. Here the term is used to include the transfer of electrons to oxidized molecular species ($D^+$ and $I_3^-$).

 This journal is © the Owner Societies 2007

routes using the equivalence

$$\upsilon_{\mathrm{inj}} = \upsilon_{\mathrm{D}^+} + \upsilon_{\mathrm{I}_3^-} - \frac{j_{\mathrm{sub}}(U_{\mathrm{photo}})}{qd} \tag{17}$$

where $d$ is the thickness of the film.

In order to simplify the treatment at this point, we assume that electron transfer to $D^+$ and electron transfer *via* the substrate can both be neglected. For homogeneous illumination, the injection rate is constant over the film and the steady state electron density is given by

$$n = \frac{\upsilon_{\mathrm{inj}}}{k_{\mathrm{I}_3^-}[\mathrm{I}_3^-]} = \upsilon_{\mathrm{inj}}\tau_n \tag{18}$$

where $\tau_n$ is the electron lifetime. It can be seen that this simple approach predicts that the steady state electron density is linearly proportional to the illumination intensity and to the electron lifetime. Clearly, one way to increase the open circuit voltage is to decrease the concentration of $I_3^-$. However, this will impose restrictions on the maximum (diffusion limited) current that the cell can deliver. The alternative is to reduce the rate constant for electron transfer by modification of the surface of the $TiO_2$ particles with blocking layers.[42,43]

If the electrons in the $TiO_2$ are free to move in the conduction band, the photovoltage can be related to the electron quasi Fermi level (or electrochemical potential) *via* the Fermi Dirac function

$$f_{\mathrm{FD}} = \frac{1}{1 + \exp\left(\frac{E - E_F}{k_{\mathrm{B}}T}\right)} \tag{19}$$

In the limit that $E - E_F$ is much greater than $k_{\mathrm{B}}T$, eqn (19) reduces to the Boltzmann limit. The density of electrons in the conduction band is determined by the product of the density of states function $N_c$ and the occupation probability, so that

$$n_c = N_C \exp\left(-\frac{E_c - {}_nE_F}{k_{\mathrm{B}}T}\right) \tag{20}$$

In the dark, the Fermi level in the $TiO_2$ is equal to the redox Fermi level, $E_{F,\mathrm{redox}}$ and the (very low) electron density is

$$n_c^0 = N_c \exp\left(-\frac{E_c - E_{F,\mathrm{redox}}}{k_{\mathrm{B}}T}\right) \tag{20b}$$

As illustrated in Fig. 8, the photovoltage is given by

$$\begin{aligned} qU_{\mathrm{photo}} &= {}_nE_F - E_{F,\mathrm{redox}} \\ &= (E_c - E_{F,\mathrm{redox}}) - (E_c - {}_nE_F) \\ &= k_{\mathrm{B}}T \ln\frac{n_c}{n_c^0} \end{aligned} \tag{21}$$

Eqn (21) shows that in order to produce a (typical) open circuit voltage of 0.77 V at 1 sun, the ratio $n_c/n_c^0$ must be $10^{13}$. Since for $E_c - E_{F,\mathrm{redox}} = 1$ eV and $N_c = 10^{21}$ cm$^{-3}$, the density of electrons in the dark is $10^4$ cm$^{-3}$, a photovoltage of 0.77 V corresponds to a free electron density of $10^{17}$ cm$^{-3}$. The rate of optical excitation at 1 sun is of the order of $10^{17}/d$ cm$^{-3}$ $= 10^{20}$ cm$^{-3}$ (typically $d$, the film thickness, $= 10$ μm). Eqn (18) shows that in order to achieve high photovoltages, the electron lifetime should be as high as possible.

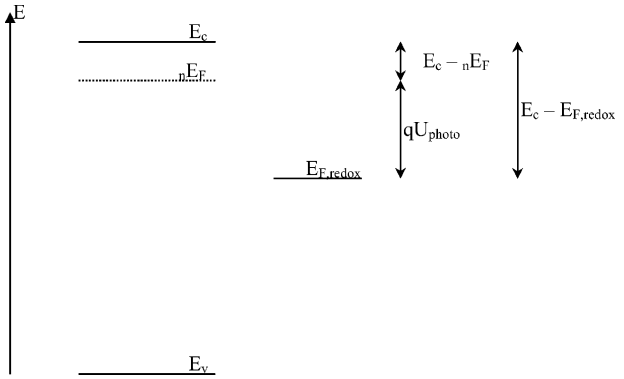


**Fig. 8** Energy diagram illustrating relationship between the terms in the expression for the photovoltage (eqn (21)).

## The IV characteristic

In order to obtain the complete IV characteristic of the DSC, we need to consider electron injection, electron transfer and electron transport. Here we make several simplifying approximations. Firstly, we neglect losses *via* electron transfer to $D^+$ and to $I_3^-$ *via* the substrate. Secondly, we neglect light scattering and treat the porous nanocrystalline electrode as optically homogeneous. Thirdly, we assume that electron transport is controlled entirely by diffusion since electrical fields normal to the substrate are negligible. Fourthly, we neglect the variations of $I_3^-$ concentration arising from the diffusion gradients set up under operating conditions. This last assumption allows us to consider the electron lifetime $\tau_n$ as independent of distance. Under steady state conditions, the generation, collection and transport of electrons is described by the continuity equation

$$\frac{\partial n}{\partial t} = \eta_{\mathrm{inj}}\alpha(\lambda)e^{-\alpha(\lambda)x} + D_n\frac{\partial^2 n_c}{\partial x^2} - \frac{n_c}{\tau_n} = 0 \tag{22}$$

The boundary conditions required for solution of this equation are

$$n_c(x = 0) = n_c^0 e^{\frac{qU}{k_{\mathrm{B}}T}} \tag{23a}$$

$$\frac{\mathrm{d}n_c}{\mathrm{d}x} = 0 \text{ at } x = d \tag{23b}$$

The current density is given by

$$j_{\mathrm{photo}} = qD_n\frac{\mathrm{d}n_c}{\mathrm{d}x} \text{ at } x = 0 \tag{24}$$

As shown by Södergren *et al.*,[44] the solution of the continuity equation can be written in a form that resembles the diode equation describing a conventional p–n photodiode.

$$j = qI_0(1 - \eta_{\mathrm{inj}}e^{-\alpha d}) - q\frac{D_0 n_c^0 d}{L_n^2}\left(e^{\frac{qU}{k_{\mathrm{B}}T}} - 1\right) \tag{25a}$$

The first term in eqn (25a) corresponds to the light-generated current. It is determined simply by the amount of light absorbed and by the injection efficiency. The second term represents the dark current of the device associated with electron transfer from the $TiO_2$ to $I_3^-$. In eqn (25a), $L_n$ is the diffusion length of electrons in the $TiO_2$, which is

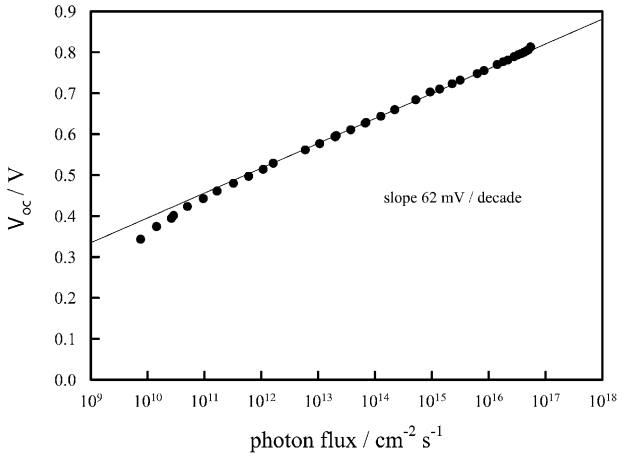


**Fig. 9** Intensity dependence of the photovoltage for a DSC with a blocking layer to prevent shunting *via* the $SnO_2$(F) substrate. The almost ideal slope indicates that the transfer of electrons to $I_3^-$ occurs predominantly *via* the conduction band of the mesoporous $TiO_2$.

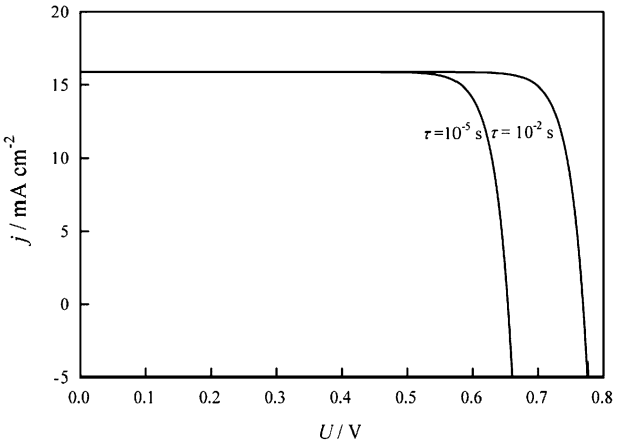


**Fig. 10** Calculated IV characteristics showing the influence of electron lifetime. Other values used in the calculation. Film thickness 10 μm, $\alpha$ = 5000 cm$^{-1}$, $N_c$ = $10^{21}$ cm$^{-3}$, $D_n$ = 0.5 cm$^2$ s$^{-1}$, $I_0$ = $10^{17}$ cm$^{-2}$ s$^{-1}$.

defined as

$$L_n = \sqrt{D_n \tau_n} \tag{25b}$$

In the limit $\exp(qU_{\text{photo}}/k_BT)$ and for strong light absorption ($e^{-\text{ad}} \ll 1$), the open circuit voltage follows from the condition $j = 0$

$$qU_{\text{photo}} = k_BT \ln\left(\frac{I_0\tau_n}{n_c^0 d}\right) = k_BT \ln\left(\frac{n_c}{n_c^0}\right) \tag{26}$$

This result is identical with the conclusion reached in the previous section.

By analogy with the conventional solid state diode, we can define the reverse saturation current density as

$$j_{\text{sat}} = q\frac{D_0 n_c^0 d}{L_n^2} = q\frac{n_c^0 d}{\tau_n} \tag{27}$$

so that the photovoltage is related to $j_{\text{sat}}$ by

$$qU_{\text{photo}} = k_BT \ln\left(\frac{qI_0}{j_{\text{sat}}}\right) \tag{28}$$

Eqn (28) illustrates the importance of minimising the reverse saturation current in order to enhance cell performance. It also predicts that the photovoltage should vary with illumination intensity with a slope of 59 mV per decade at 300 K (ideal diode behaviour). Fig. 9 shows that an optimized DSC does indeed behave almost as predicted by eqn (28)¶¶.

Solution of the continuity equation as a function of voltage $U$ between $U = 0$ and $U = U_{\text{photo}}$ gives the complete IV characteristic as illustrated in Fig. 10 for two different values of the electron lifetime.

### The electron quasi Fermi level in the DSC

Solution of the continuity equation also gives the profiles of electron density under operating conditions. Fig. 11a illustrates the profile of electron concentration under short circuit conditions calculated for monochromatic illumination corresponding approximately to 1 sun. The corresponding variation of the electron quasi Fermi level, ${}_nE_F$, is shown in Fig. 11b. The result is interesting because the difference in ${}_nE_F$ between $x = 0$ and $x = d$ is predicted to be of the order of 0.5 eV. Fig. 11b also shows the driving force corresponding to the gradient of ${}_nE_F$. It is high near the contact because the concentration of electrons is low.

By contrast with the situation at short circuit, the electron density (and hence electron quasi Fermi level under open circuit conditions) is almost constant across the entire film, and the difference ${}_nE_F - E_{F,\text{redox}}$ determines the photovoltage measured at the contacts. The continuity equation can be solved for voltages between $U = 0$ and $U > U_{\text{photo}}$, and the results are shown in Fig. 12, which shows how the value of ${}_nE_F$ at $x = d$ (other side of the film) varies along the IV characteristic.

The predictions of the model presented here have been tested recently using a DSC in which an evaporated titanium electrode is used to sense the quasi Fermi level at $x = d$.[45] The titanium electrode is passivated by air oxidation to ensure that it does not provide a shunt path for electrons in the $TiO_2$. The cell design is illustrated in Fig. 13 together with the experimentally measured variation of the quasi Fermi level at $x = d$. It can be seen that the experiment results agree with Fig. 12.

If the electron lifetime is short, electrons will be lost during transit to the contact. This problem is particularly acute when the $I_3^-/I^-$ redox system is replaced by one-electron redox systems[46] or by hole conducting organic materials such as spiro(MeOTAD).[36,47,48] The effect on the profile of electrons under short circuit conditions for illumination from the substrate side is shown in Fig. 14a. If the gradient of electron density in the bulk of the film becomes negative, electrons diffuse away from the contact to be lost by electron transfer to the redox species. If this occurs, only the region of the film adjacent to the contact is active in generating photocurrent.

A useful figure of merit in this context is the electron diffusion length. The fraction of injected electrons that will be collected from 10 μm $TiO_2$ film depends on the electron

¶¶ Non-ideal diode behaviour is frequently reported for DSCs. Possible reasons for non-ideality include shunting *via* the substrate and electron transfer *via* surface states.

 This journal is © the Owner Societies 2007

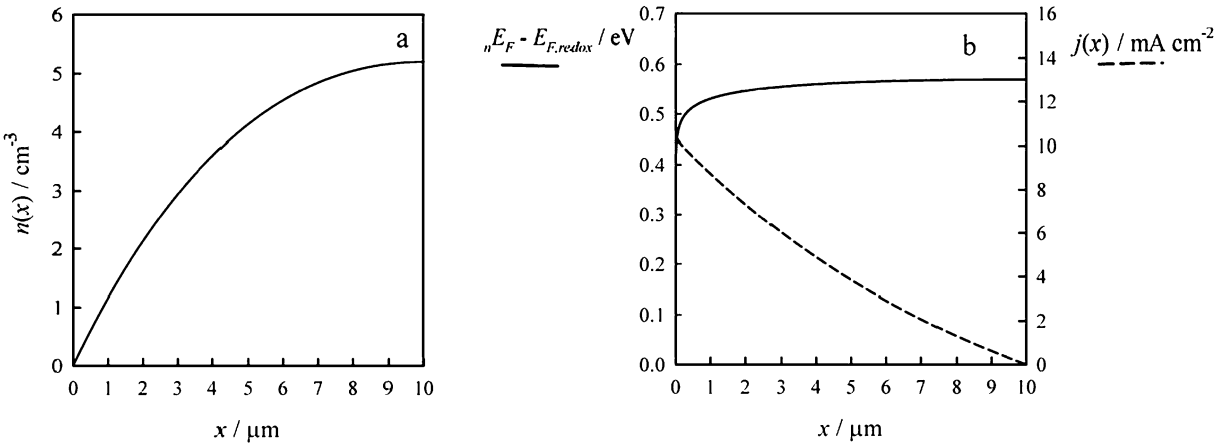


**Fig. 11** (a) Calculated profile of free electron density under short circuit conditions. (b) Corresponding profile of the electron quasi Fermi level (continuous line) and of the local current density calculated from eqn (2) (broken line). Values used in the calculation: $I_0 = 10^{17}$ cm$^{-2}$ s$^{-1}$, $d =$ 10 μm, $\alpha = 1000$ cm$^{-1}$, $D_n = 0.5$ cm$^2$ s$^{-1}$, $E_c - E_{F,\mathrm{redox}} = 1.0$ eV.

diffusion length as shown in Fig. 14b. It is evident that optimum performance is obtained when the electron diffusion length is several times greater than the film thickness.

### Voltage losses in the DSC

In an operating DSC, it is necessary to consider several loss mechanisms apart from those mentioned above. The IV characteristics will not be described by eqn (25a) because the transfer of electrons to $I_3^-$ at the cathode requires a finite driving voltage ('overpotential'). The current density at the cathode is described by the Butler Volmer equation[39] which can be written as

$$j = zqk^0\left[n_R^\sigma e^{\frac{(1-\alpha)zq(E-E^0)}{k_\mathrm{B}T}} - n_O^\sigma \exp^{-\frac{\alpha zq(E-E^0)}{k_\mathrm{B}T}}\right] \qquad (29)$$

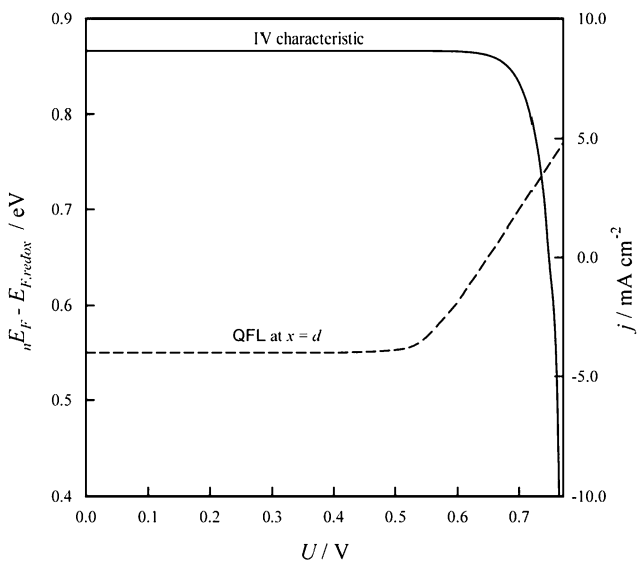


**Fig. 12** Calculated variation of the electron quasi Fermi level (QFL) at $x = d$ along the IV plot. Note that the QFL remains constant over a voltage range of 0.5 V from short circuit, before rising as electron accumulation begins at more negative voltages. Values used in the calculation. $I_0 = 10^{17}$ cm$^{-2}$ s$^{-1}$, $\tau_n = 5 \times 10^{-5}$ s, $D_n = 0.5$ cm$^2$ s$^{-1}$. $d = 5$ μm, $\alpha = 1000$ cm$^{-1}$.

Here $k_0$ is the standard rate constant for the electron transfer reaction, $n_R^\sigma$ and $n_\mathrm{O}^\sigma$ are the densities of $I^-$ and $I_3^-$ at the cathode surface, respectively, $z$ is the number of electrons transferred and $\alpha$ is the cathodic transfer coefficient. The upper limit of the cell current at high light intensities (generally $>1$ sun) is determined by diffusion of $I_3^-$ to the cathode under conditions where the $I_3^-$ is completely depleted at the cathode surface.

$$j_{\mathrm{lim},c} = 2qD_{I_3^-}\left.\frac{\mathrm{d}n_{I_3^-}}{\mathrm{d}x}\right|_{x=0} = 4qD_{I_3^-}\frac{n_{I_3^-,\mathrm{bulk}}}{\mathrm{d}} \qquad (30)$$

The current density at lower light intensities will be determined by electron transfer and diffusion (mixed control), and the current voltage relationship becomes

$$\frac{j}{j_0} = \left(1 - \frac{j}{j_{\mathrm{lim},a}}\right)e^{\frac{(1-\alpha)zq\eta}{kT}} - \left(1 - \frac{j}{j_{\mathrm{lim},c}}\right)e^{-\frac{\alpha zq\eta}{kT}} \qquad (31)$$

where $\eta$ is the overpotential, *i.e.* the difference between the electrode potential and its equilibrium (Nernstian) value.

Fig. 15 shows how the overvoltage at the cathode varies with current density for typical values of the rate constant and concentrations. At a current density of 15 mA cm$^{-2}$, the losses will be a only a few tens of millivolts if a platinum coated cathode is used. However, less active cathode materials with lower values of the electron transfer rate constant $k^0$ will give large voltage losses‖ ‖.

The voltage loss associated with driving the reduction of $I_3^-$ at the cathode will be seen on the IV characteristic as degradation of the fill factor, which is defined as the maximum power output divided by the product of the short circuit current and open circuit voltage.

$$FF = \frac{j_\mathrm{mp}V_\mathrm{mp}}{j_\mathrm{sc}V_\mathrm{oc}} \qquad (32)$$

‖ ‖ Platinum is an electrocatalyst for the iodide/tri-iodide redox couple. Iodine is dissociatively chemisorbed on platinum, overcoming the high activation energy associated with breaking the I–I bond. The DSC therefore relies on electron transfer to $I_3^-$ being very fast at platinum but very slow at the mesoporous $TiO_2$. In the absence of this 'kinetic asymmetry', the cell does not work.

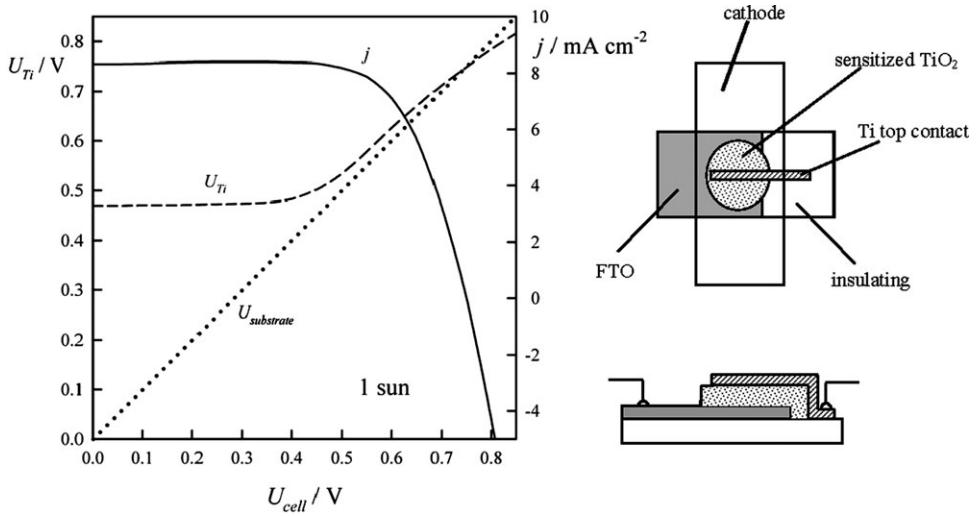


**Fig. 13** Experimental variation of the electron QFL at $x = d$ measured using a titanium indicator electrode evaporated on the top of the mesoporous $TiO_2$ layer. Compare with Fig. 12. The construction of the cell with a titanium top electrode is illustrated on the right (see ref. 35 for details).

The open circuit voltage is not affected, since no current flows at $V_{oc}$ and therefore the voltage loss at the cathode is zero. Fig. 16 shows how the cathode voltage loss affects the IV characteristic.

So far we have neglected the losses associated with electron transfer at the substrate (*cf.* eqn (17)). This 'shunting' mechanism is particularly important for cells in which the $I_3^-/I^-$ redox couple is replaced with a one electron transfer couple such as Co(III)/Co(II)(dbbip)(2) (dbbip = 2,6-bis(1′-butylbenzimidazol-2′-yl) pyridine)[49,50] or in cells with an organic hole conductor such as spiro(MeOTAD).[36,48] At high intensities (1 sun), substrate shunting is less important for cells using the $I_3^-/I^-$ redox system.[40] For cells using alternative electrolytes or organic hole conductors, a thin ($\cong$50 nm) blocking layer of compact $TiO_2$ is necessary to prevent severe degradation of cell performance by shunting. The characteristics of the blocking layer can be examined using thin layer cells without the mesoporous $TiO_2$ layer.[51] Fig. 17 illustrates how effective the blocking layer can be in reducing losses due to electron transfer from the substrate. Electron transfer *via* the substrate can also be identified by measuring the open circuit photovoltage decay. Cells with good blocking layers to suppress the back reaction exhibit remarkably slow photovoltage decays over a period of up to one hour.[52]

### Electron transport and trapping in the DSC

The preceding discussion has focussed on the steady state behaviour of the DSC. The responses of the cell voltage and current to changes in light intensity reveal that electrons are

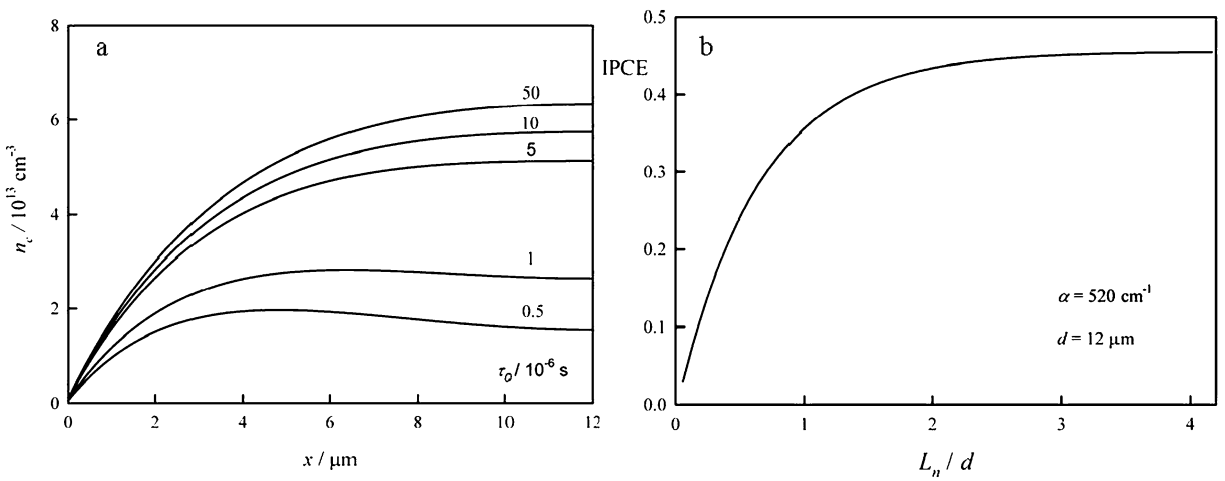


**Fig. 14** Profiles of electron density under short circuit conditions showing the effect of reducing the free electron lifetime. (a) Dependence of the incident photon to current conversion efficiency (IPCE) on the ratio of the electron diffusion length $L_n$ to the film thickness, $d$. Note that for $L_n/d > 3$ the IPCE approaches its limiting value, which is determined by the fraction of incident light absorbed by the film (in this case 45%). Values used in calculation. $\alpha = 1000$ cm$^{-1}$, $d = 10$ μm, $D_n = 0.5$ cm$^2$ s$^{-1}$.

 This journal is © the Owner Societies 2007

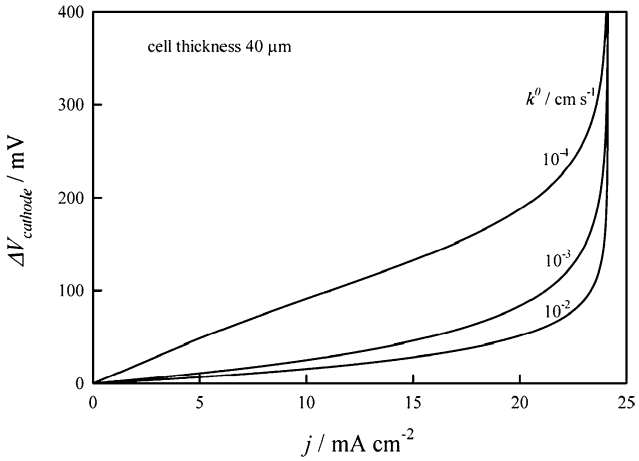


**Fig. 15** Plots showing how the voltage loss at the cathode in a DSC depends on current density and on $k^0$, the rate constant for the electron transfer process. In the limit that $k^0$ is greater than 0.1 cm s$^{-1}$, as one would expect for a highly active cathode material, the voltage loss is determined entirely by diffusion ('diffusion overvoltage'). Lower values of $k^0$ lead to larger voltage losses arising from the 'kinetic overpotential'.

trapped at states located in the bandgap of the oxide as shown in the upper part of Fig. 18. Electron transport to the contact involves multiple trapping events as illustrated in the lower part of Fig. 18. This process can be modelled as a random walk on a lattice with a distribution of waiting times[53] or as trapping and thermal release of electrons from states distributed in energy.[54–57] The process has also been modelled using Monte Carlo methods in order to examine the effect of morphology on electron percolation.[58,59]

In general, the density of electrons in the conduction band is many orders of magnitude lower than the density of trapped electrons. Although electron transport and electron transfer involve conduction band electrons, dynamic measurements of

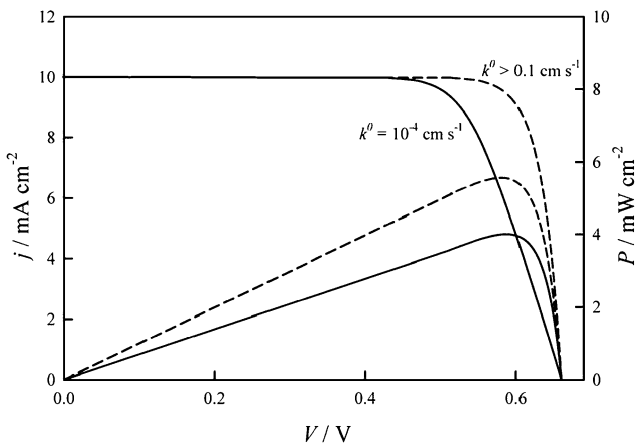


**Fig. 16** Calculated IV plots showing the influence of sluggish electron transfer kinetics at the DSC cathode. Note that the short circuit current and open circuit voltage are unaffected by low values of $k^0$, but the fill factor is adversely affected, as can be seen from the difference between the power plots for fast (broken line) and slow (solid line) electron transfer.

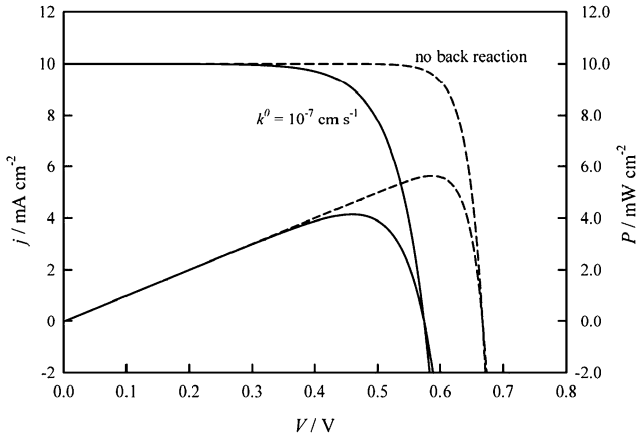


**Fig. 17** IV plots showing the influence of shunting *via* the $SnO_2$(F) substrate. Even for a relatively low value of the electron transfer rate constant ($k^0 = 10^{-7}$ cm s$^{-1}$), the loss of open circuit voltage and maximum power output can be significant.

photocurrent and photovoltage are strongly influenced by trapping/detrapping since the trap occupation responds to changes in the density of electrons in the conduction band. This means, for example, that the true electron lifetime is not accessible from transient photovoltage measurements. Similarly, the true diffusion coefficient of electrons cannot be derived directly from transient photocurrent measurements. This has important implications for attempts to determine these quantities as part of a strategy for cell optimization. Methods used to determine the relaxation times associated

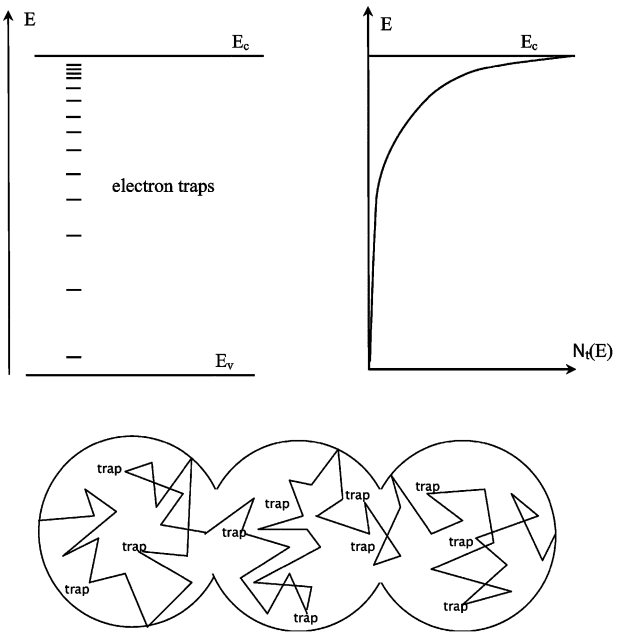


**Fig. 18** Electron trap states in the $TiO_2$ appear to be distributed exponentially in energy as shown in the upper part of the figure. Here $N_t(E)$ is the density of states of the traps. Electron transport in the $TiO_2$ particles involves multiple trapping events as shown in the lower part of the figure. The dynamic response of the DSC is strongly influenced by trapping/detrapping of electrons.

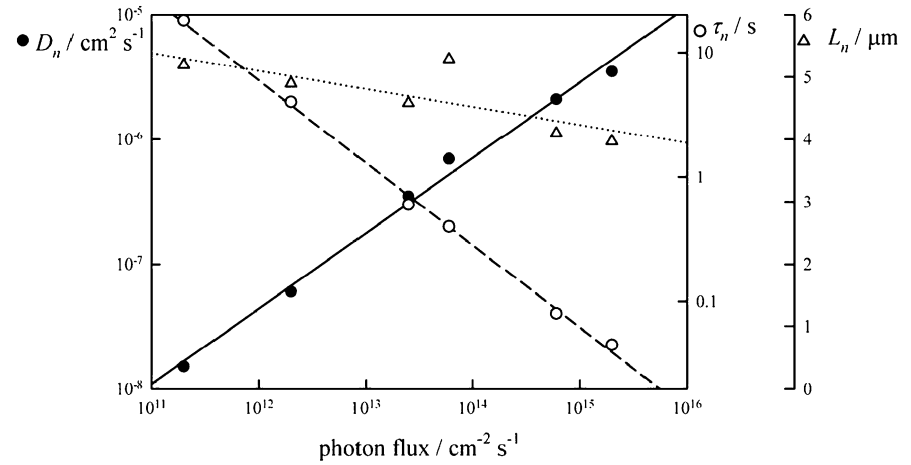


**Fig. 19** Intensity dependence of the apparent values of the electron diffusion coefficient and electron lifetime measured for a MeOTAD cell (data from ref. 28). The intensity dependence arises from the influence of electron trapping/detrapping on the dynamic photocurrent and photovoltage responses. The figure also shows the calculated electron diffusion length, which varies only weakly with light intensity as predicted theoretically by the multiple trapping model.

with recombination and transport in DSCs include small amplitude transient[60–63] and periodic[64–67] methods.

In order to treat the non steady state situation, the continuity equation (eqn (22)) must be modified to include terms to account for trapping and detrapping of electrons. A very clear treatment of this problem has been given by Bisquert and Vikhrenko,[68] who have shown that the apparent values of the electron diffusion coefficient, $D_n$, and electron lifetime, $\tau_n$, are related to the true (conduction band) values $D_0$ and $\tau_0$ by

$$D_n = \left(\frac{\partial n_c}{\partial n_t}\right) D_0 \quad \text{and} \quad \tau_n = \left(\frac{\partial n_t}{\partial n_c}\right) \tau_0 \tag{33}$$

It follows that

$$L_n = \sqrt{D_0 \tau_0} = \sqrt{D_n \tau_n} \tag{34}$$

The $\left(\frac{\partial n_c}{\partial n_t}\right)$ and $\left(\frac{\partial n_t}{\partial n_c}\right)$ terms in eqn (33) can be found by noting that

$$\frac{\partial n_t}{\partial n_c} = \frac{\partial n_t}{\partial_n E_F} \frac{\partial_n E_F}{\partial n_c} = g(E) \frac{k_B T}{n_c} \tag{35}$$

Here $g(E)$ is the density of states distribution from the electron traps*** (methods that provide information about trap distributions include photovoltage decay[52,69] and charge extraction[52,70]).

An important consequence of the relationships above is that $D_n$ and $\tau_n$ depend on trap occupancy and therefore on illumination intensity, but their product does not, so that $L_n$ remains constant and is accessible to measurement *via* determination of $D_n$ and $\tau_n$. This means that determination of $L_n$ is possible in principle, even if $D_0$ and $\tau_0$ are not accessible individually. For an exponential distribution of traps, $D_n$ and $\tau_n$ vary with intensity according to a power law with opposite sign as illustrated in Fig. 19 for the case of a spiro-MeOTAD cell.[37] In this case, the experimentally determined diffusion length varies by less than 30% over the entire range of intensity.

*** Experimentally determined trap distributions in $TiO_2$ commonly follow an exponential energy distribution, with the number of traps tailing off as the energy moves down into the bandgap.

## Conclusions and outlook

Development of new types of dye-sensitized solar cells and the optimization of existing types involves consideration of all electron transport and electron transfer processes, not just those taking place in the mesoporous layer. The modelling of cell characteristics using the continuity equation provides a useful starting point for understanding the factors that control the efficiency of charge collection and voltage generation. Key parameters that control device performance include band edge positions, electron diffusion coefficients and rate constants for interfacial electron transfer. More work is required to understand how to control these parameters, for example by self-assembly and surface modification. The influence of trapping/detrapping on the DSC response remains a controversial question, with several recent papers claiming that the multiple trapping model may not be correct,[71,72] and other supporting it.[73,74] In any case, the identity of the trapping states remains unclear as does the existence and possible role of surface states.

The future development of this exciting field will need to combine novel approaches to materials design with appropriate modelling of the various cell components. Key challenges include demonstration of device stability and scale-up of fabrication. It seems unlikely that an acceptable lifetime will be achievable using liquid redox mediators, and more work is needed to identify and optimize alternative 'hole conducting' media that are cheap and stable. Even leaving aside the still open question of its eventual commercial exploitation, the DSC is likely to remain a powerful stimulus for new materials chemistry and theoretical modelling.

 This journal is © the Owner Societies 2007

## Glossary of symbols

| | |
|---|---|
| $\alpha$ | Absorption coefficient or cathodic transfer coefficient/cm$^{-1}$ |
| $c$ | Concentration/mol dm$^{-3}$ |
| $d$ | Film thickness/cm |
| $D_0$ | Diffusion coefficient of free electrons/cm$^2$ s$^{-1}$ |
| $D_n$ | Apparent (trap controlled) electron diffusion coefficient/cm$^2$ s$^{-1}$ |
| $\Delta\phi$ | Potential difference across space charge region of a semiconductor/V |
| $E$ | Electrode potential/V or energy/eV |
| $E^0$ | standard electrode potential/V |
| $E_c$ | Conduction band energy/eV |
| $E_F$ | Fermi energy/eV |
| ${}_nE_F$ | quasi Fermi energy/eV |
| $E_{F,\mathrm{redox}}$ | Redox Fermi energy/eV |
| $\varepsilon$ | Relative permittivity (dimensionless) |
| $\varepsilon_0$ | Permittivity of vacuum/F cm$^{-1}$ |
| $f_{\mathrm{FD}}$ | Fermi Dirac function (dimensionless) |
| FF | Fill factor (dimensionless) |
| $\phi$ | Electrostatic potential/V |
| $g(E)$ | Density of states function for electron traps/ cm$^{-3}$ eV$^{-1}$ |
| $\eta$ | Overpotential for an electrode process/V |
| $\eta_{\mathrm{inj}}$ | Injection efficiency of sensitization process |
| $I_0$ | Incident photon flux/cm$^{-2}$ s$^{-1}$ |
| $j$ | Current density/A cm$^{-2}$ |
| $j^0$ | Exchange current density for an electrode reaction/ A cm$^{-2}$ |
| $j_{\mathrm{lim},a}$ | Diffusion limited anodic current density/A cm$^{-2}$ |
| $j_{\mathrm{lim},c}$ | Diffusion limited cathodic current density/A cm$^{-2}$ |
| $j_{\mathrm{photo}}$ | Photocurrent density/A cm$^{-2}$ |
| $j_{sc}$ | Short circuit current density/A cm$^{-2}$ |
| $j_{\mathrm{sub}}$ | Current density at substrate |
| $j^0_{\mathrm{sub}}$ | Exchange current density at substrate |
| $J_i$ | Flux of species $i$/cm$^{-2}$ s$^{-1}$ |
| $K$ | Rate constant for a volume process/s$^{-1}$ |
| $k_{\mathrm{B}}$ | Boltzmann constant/eV K$^{-1}$ |
| $k^0$ | Standard heterogeneous rate constant for electron transfer/cm s$^{-1}$ |
| $L_n$ | Electron diffusion length/cm |
| $\lambda$ | Wavelength/nm |
| $\bar{\mu}_i$ | Electrochemical potential of species $i$ |
| $\mu_i^0$ | Standard chemical potential of species $i$ |
| $n_c$ | Conduction band electron density/cm$^{-3}$ |
| $n_c^0$ | Equilibrium (dark) conduction band electron density/cm$^{-3}$ |
| $n_i$ | Number density of particles $i$/cm$^{-3}$ |
| $n_t$ | Density of trapped electrons/cm$^{-3}$ |
| $N_d$ | Donor density/cm$^{-3}$ |
| $q$ | Elementary charge/C |
| $T$ | Absolute temperature/K |
| $\tau_0$ | Conduction band electron lifetime/s |
| $\tau_n$ | Apparent (trap controlled) electron lifetime/s |
| $u_i$ | Mobility of species I/cm$^2$ V$^{-1}$ s$^{-1}$ |
| $U$ | Voltage/V |
| $U_{\mathrm{photo}}$ | Photovoltage/V |
| $\upsilon$ | Volume rate of a process/cm$^{-3}$ s$^{-1}$ |
| $V_{\mathrm{oc}}$ | Open circuit voltage/V |
| $W_{\mathrm{sc}}$ | Width of space charge region/cm |
| $z$ | Number of electrons transferred in an electrode reaction |
| $z_i$ | Charge number of species $i$ (dimensionless) |


## Acknowledgements

The author thanks all past and present members of his research group, who obtained the experimental results described in this article, as well as Alison Walker for endless helpful discussions and Jonnie Williams for the numerical simulation of Fig. 6. This work has been supported by the EPSRC SUPERGEN programme (Excitonic Solar Cell Consortium).


## References


1 http://astsun.astro.virginia.edu/~rjp0i/museum/photography.html.
2 M. Grätzel, *Nature*, 2001, **414**, 338–344.
3 H. Gerischer and H. Tributsch, *Ber. Bunsen-Ges. Phys. Chem.*, 1966, **72**, 437–445.
4 K. Hauffe, H. J. Danzmann, H. Pusch, J. Range and H. Volz, *J. Electrochem. Soc.*, 1970, **117**, 993–999.
5 H. Tsubomura, M. Matsamura, Y. Noyamura and T. Amamyiaya, *Nature*, 1976, **261**, 402.
6 B. O'Regan and M. Grätzel, *Nature*, 1991, **353**, 737–740.
7 M. Gratzel, *C. R. Chim.*, 2006, **9**, 578–583.
8 M. Zukalova, A. Zukal, L. Kavan, M. K. Nazeeruddin, P. Liska and M. Grätzel, *Nano Lett.*, 2005, **5**, 1789–1792.
9 M. D. Wei, Y. Konishi, H. S. Zhou, M. Yanagida, H. Sugihara and H. Arakawa, *J. Mater. Chem.*, 2006, **16**, 1287–1293.
10 K. Hara, M. Kurashige, Y. Dan-oh, C. Kasada, A. Shinpo, S. Suga, K. Sayama and H. Arakawa, *New J. Chem.*, 2003, **27**, 783–785.
11 K. Hara, T. Sato, R. Katoh, A. Furube, T. Yoshihara, M. Murai, M. Kurashige, S. Ito, A. Shinpo, S. Suga and H. Arakawa, *Adv. Funct. Mater.*, 2005, **15**, 246–252.
12 S. L. Li, K. J. Jiang, K. F. Shao and L. M. Yang, *Chem. Commun.*, 2006, 2792–2794.
13 K. R. J. Thomas, J. T. Lin, Y. C. Hsu and K. C. Ho, *Chem. Commun.*, 2005, 4098–4100.
14 S. Yanagida, *C. R. Chim.*, 2006, **9**, 597–604.
15 G. Dennler and N. S. Sariciftci, *Proc. IEEE*, 2005, **93**, 1429–1439.
16 S. E. Gledhill, B. Scott and B. A. Gregg, *J. Mater. Res.*, 2005, **20**, 3167–3179.
17 H. Spanggaard and F. C. Krebs, *Sol. Energy Mater.*, 2004, **83**, 125–146.
18 H. Hoppe and N. S. Sariciftci, *J. Mater. Res.*, 2004, **19**, 1924–1945.
19 C. Sanchez, B. Julian, P. Belleville and M. Popall, *J. Mater. Chem.*, 2005, **15**, 3559–3592.
20 H. W. Han, W. Liu, J. Zhang and X. Z. Zhao, *Adv. Funct. Mater.*, 2005, **15**, 1940–1944.
21 D. Gebeyehu, C. J. Brabec and N. S. Sariciftci, *Thin Solid Films*, 2002, **403**, 271–274.
22 M. Gratzel, *Chem. Lett.*, 2005, **34**, 8–13.
23 A. Duret and M. Gratzel, *J. Phys. Chem. B*, 2005, **109**, 17184–17191.
24 M. K. Nazeeruddin, A. Kay, I. Rodicio, R. Humphrybaker, E. Muller, P. Liska, N. Vlachopoulos and M. Grätzel, *J. Am. Chem. Soc.*, 1993, **115**, 6382–6390.
25 M. K. Nazeeruddin, R. Humphry-Baker, P. Liska and M. Gratzel, *J. Phys. Chem. B*, 2003, **107**, 8981–8987.

26 T. Horiuchi, H. Miura and S. Uchida, *Chem. Commun*., 2003, 3036–3037.
27 T. Horiuchi, H. Miura and S. Uchida, *J. Photochem. Photobiol., A*, 2004, **164**, 29–32.
28 J. E. Moser, M. Wolf, F. Lenzmann and M. Grätzel, *Z. Phys. Chem*., 1999, **212**, 85–92.
29 B. Burfeindt, C. Zimmermann, S. Ramakrishna, T. Hannappel, B. Meissner, W. Storck and F. Willig, *Z. Phys. Chem*., 1999, **212**, 67–75.
30 Y. Tachibana, J. E. Moser, M. Grätzel, D. R. Klug and J. R. Durrant, *J. Phys. Chem*., 1996, **100**, 20056–20062.
31 Y. Wang, J. B. Asbury and T. Lian, *J. Phys. Chem. A*, 2000, **104**, 4291–4299.
32 J. Nelson and R. E. Chandler, *Coord. Chem. Rev*., 2004, **248**, 1181–1194.
33 P. Wang, B. Wenger, R. Humphry-Baker, J. E. Moser, J. Teuscher, W. Kantlehner, J. Mezger, E. V. Stoyanov, S. M. Zakeeruddin and M. Grätzel, *J. Am. Chem. Soc*., 2005, **127**, 6850–6856.
34 S. Y. Huang, G. Schlichthorl, A. J. Nozik, M. Grätzel and A. J. Frank, *J. Phys. Chem. B*, 1997, **101**, 2576–2582.
35 P. Würfel, *Physics of Solar Cells*, Wiley-VCH, Weinheim, 2005.
36 U. Bach, D. Lupo, P. Comte, J. E. Moser, F. Weissortel, J. Salbeck, H. Spreitzer and M. Grätzel, *Nature*, 1998, **395**, 583–585.
37 J. Kruger, R. Plass, M. Grätzel, P. J. Cameron and L. M. Peter, *J. Phys. Chem. B*, 2003, **107**, 7536–7539.
38 A. N. M. Green, R. E. Chandler, S. A. Haque, J. Nelson and J. R. Durrant, *J. Phys. Chem. B*, 2005, **109**, 142–150.
39 A. J. Bard and L. R. Faulkner, *Electrochemical Methods: Fundamentals and Applications*, John Wiley and Sons Inc., New York, 2nd edn, 2001.
40 P. J. Cameron, L. M. Peter and S. Hore, *J. Phys. Chem. B*, 2005, **109**, 930–936.
41 P. J. Cameron and L. M. Peter, *J. Phys. Chem. B*, 2005, **109**, 7392–7398.
42 J. Spivack, T. Siclovan, S. Gasaway, E. Williams, A. Yakimov and J. Gui, *Sol. Energy Mater*., 2006, **90**, 1296–1307.
43 E. Palomares, J. N. Clifford, S. A. Haque, T. Lutz and J. R. Durrant, *J. Am. Chem. Soc*., 2003, **125**, 475–482.
44 S. Södergren, A. Hagfeldt, J. Olsson and S. E. Lindquist, *J. Phys. Chem*., 1994, **98**, 5552–5555.
45 K. P. Lobato, L. M. Peter and U. Würfel, *J. Phys. Chem. B*, 2006, **110**, 16201.
46 B. A. Gregg, F. Pichot, S. Ferrere and C. L. Fields, *J. Phys. Chem. B*, 2001, **105**, 1422.
47 R. Plass, S. Pelet, J. Krueger, M. Grätzel and U. Bach, *J. Phys. Chem. B*, 2002, **106**, 7578–7580.
48 J. Kruger, R. Plass, L. Cevey, M. Piccirelli, M. Grätzel and U. Bach, *Appl. Phys. Lett*., 2001, **79**, 2085–2087.
49 H. Nusbaumer, J. E. Moser, S. M. Zakeeruddin, M. K. Nazeeruddin and M. Grätzel, *J. Phys. Chem. B*, 2001, **105**, 10461–10464.
50 P. J. Cameron, L. M. Peter, S. M. Zakeeruddin and M. Grätzel, *Coord. Chem. Rev*., 2004, **248**, 1447–1453.
51 P. J. Cameron and L. M. Peter, *J. Phys. Chem. B*, 2003, **107**, 14394–14400.
52 M. Bailes, P. J. Cameron, K. Lobato and L. M. Peter, *J. Phys. Chem. B*, 2005, **109**, 15429–15435.
53 J. Nelson, *Phys. Rev. B: Condens. Matter*, 1999, **59**, 15374–15380.
54 A. C. Fisher, L. M. Peter, E. A. Ponomarev, A. B. Walker and K. G. U. Wijayantha, *J. Phys. Chem. B*, 2000, **104**, 949–958.
55 J. Bisquert, A. Zaban and P. Salvador, *J. Phys. Chem. B*, 2002, **106**, 8774–8782.
56 L. M. Peter, E. A. Ponomarev, G. Franco and N. J. Shaw, *Electrochim. Acta*, 1999, **45**, 549–560.
57 L. M. Peter, N. W. Duffy, R. L. Wang and K. G. U. Wijayantha, *J. Electroanal. Chem*., 2002, **524**, 127–136.
58 M. J. Cass, F. L. Qiu, A. B. Walker, A. C. Fisher and L. M. Peter, *J. Phys. Chem. B*, 2003, **107**, 113–119.
59 M. J. Cass, A. B. Walker, D. Martinez and L. M. Peter, *J. Phys. Chem. B*, 2005, **109**, 5100–5107.
60 N. Kopidakis, E. A. Schiff, N. G. Park, J. van de Lagemaat and A. J. Frank, *J. Phys. Chem. B*, 2000, **104**, 3930–3936.
61 N. W. Duffy, L. M. Peter and K. G. U. Wijayantha, *Electrochem. Commun*., 2000, **2**, 262–266.
62 N. Kopidakis, K. D. Benkstein, J. van de Lagemaat and A. J. Frank, *J. Phys. Chem. B*, 2003, **107**, 11307–11315.
63 J. van de Lagemaat and A. J. Frank, *J. Phys. Chem. B*, 2000, **104**, 4292–4294.
64 G. Schlichthörl, S. Y. Huang, J. Sprague and A. J. Frank, *J. Phys. Chem. B*, 1997, **101**, 8141–8155.
65 L. Dloczik, O. Ileperuma, I. Lauermann, L. M. Peter, E. A. Ponomarev, G. Redmond, N. J. Shaw and I. Uhlendorf, *J. Phys. Chem. B*, 1997, **101**, 10281–10289.
66 L. M. Peter and D. Vanmaekelbergh, in *Adv. Electrochem. Sci. Eng*., Weinheim, 1999, vol. 6, pp. 77–163.
67 G. Schlichthörl, N. G. Park and A. J. Frank, *J. Phys. Chem. B*, 1999, **103**, 782–791.
68 J. Bisquert and V. S. Vikhrenko, *J. Phys. Chem. B*, 2004, **108**, 2313–2322.
69 A. Zaban, M. Greenshtein and J. Bisquert, *ChemPhysChem*, 2003, **4**, 859–864.
70 N. W. Duffy, L. M. Peter, R. M. G. Rajapakse and K. G. U. Wijayantha, *Electrochem. Commun*., 2000, **2**, 658–662.
71 G. Boschloo and A. Hagfeldt, *J. Phys.Chem. B*, 2005, **109**, 12093–12098.
72 N. Kopidakis, K. D. Benkstein, J. van de Lagemaat, A. J. Frank, Q. Yuan and E. A. Schiff, *Phys. Rev. B*, 2006, **73**.
73 L. M. Peter, A. B. Walker, G. Boschloo and A. Hagfeldt, *J. Phys. Chem. B*, 2006, **110**, 13694–13699.
74 K. Lobato and L. M. Peter, *J. Phys. Chem. B*, 2006, **110**, 21920–21923.


 This journal is © the Owner Societies 2007